Electronic Supplementary Material (ESI) for CrystEngComm.

Supporting Information

Assembly of a rod indium-organic framework with fluorescence property for selective sensing of Cu^{2+}, Fe^{3+} and nitroaromatics in water

Hao Zhang, Zi-Jun Ding, Yu-Hui Luo,* Wu-Yue Geng, Zhi-Xuan Wang, Dong-En Zhang*

School of Environmental and Chemical Engineering, Jiangsu Ocean University, Lianyungang 222000, P. R. China.

* Corresponding authors. E-mail: luoyh@jou.edu.cn (Yu-Hui Luo);
2007000040@jou.edu.cn (Dong-En Zhang)

Materials and Measurements

All reagents and solvents were purchased from commercial sources and used without purification. TCA was prepared according to the literature[1]. Powder X-ray diffraction (PXRD) patterns was collected on a PANalytical X'Pert Powder X-ray diffractometer with graphite monochromatized Cu $K\alpha$ radiation (λ = 0.15418 nm), 2θ ranging from 5 to 50 ^{o} with an increment of 0.02 ^{o}, and a scanning rate of 10 ^{o}/min. The FT-IR spectra was measured by using KBr pellets in the range 4000 - 500 cm^{-1} on a Thermo Scientific spectrometer. The UV-Vis absorption was measured with a PERSEE UV-Vis-NIR spectrophotometer. The fluorescent spectroscopy was measured on a FL-7000 HITACHI luminescence spectrometer at room temperature with a light source of Xenon lamp.

X-ray crystallography

Crystallographic diffraction data for **JOU-25** was recorded on a Bruker Apex CCD diffractometer with graphite monochromatized Mo-$K\alpha$ radiation (λ = 0.71073 Å) at room temperature. **JOU-25** was solved by Direct Method of SHELXS-2018 and refined by full-matrix least-squares technique by using the SHELXL-2018 program[2]. All nonhydrogen atoms were refined with anisotropic temperature parameters. All hydrogen atoms were placed in geometrically idealized position as a riding mode. The solvent molecules in the crystal are highly disordered and are removed by using the SQUEEZE routine of PLATON[3]. For **JOU-25-R**, SADI, DFIX, SIMU, ISOR and FLAT commands were used to restrict some of the atoms and bond length, whereas AFIX 66 was used to restrict the geometry of benzene ring of the ligand. For **JOU-25-S**, DFIX, SIMU and ISOR commands were used to restrict some of the atoms and bond length, whereas AFIX 66 was used to restrict the geometry of benzene ring of the ligand. For both **JOU-25-R** and **JOU-25-S**, PLAT420_ALERT_2_B may be due to the following reasons. The solvent molecules may be the acceptors of this O-H bonds, but the solvent molecules are highly disordered and removed using the SQUEEZE routine of PLATON. For **JOU-25-S**, although the crystallographic data have been recorded twice and Twin/BASF commands have been added, a relative high flack value was obtained, resulting in PLAT987_ALERT_1_B. PLAT342_ALERT_3_B may be due to the bad quality of the crystal. The crystallographic data for **JOU-25** was summarized in Table S1, and the selected bond lengths and angles are listed in Table S2 and S3. CCDC numbers for **JOU-25-R** and **JOU-25-S** are 2103362 and 2103363, respectively.

Table S1. Crystallographic data and structure refinements of **JOU-25**.

Compounds	**JOU-25-R**	**JOU-25-S**
Formula	$C_{87}H_{64}In_5N_5O_{31}$	$C_{87}H_{64}In_5N_5O_{31}$
Formula weight	2249.53	2249.53
Crystal system	hexagonal	hexagonal
Space group	$P6_1$	$P6_5$
a (Å)	37.5060(8)	37.662(5)
b (Å)	37.5060(8)	37.662(5)
c (Å)	16.9308(7)	17.189(2)

α (°)	90	90
β (°)	90	90
γ (°)	120	120
V (Å^3)	20625.7(12)	21115(6)
Z	6	6
Density (g cm^{-3})	1.087	1.061
μ / mm^{-1}	0.881	0.861
F(000)	6384	6684
2θ (°)	4.466 - 50.485	4.901 - 50.565
Reflections	273224	115846
Data/restraints/parameters	31574/1305/1076	24522/2797/1052
GOF on F^2	1.040	1.049
R_1, wR_2 [I > 2σ (I)]	0.0322, 0.0831	0.0891, 0.2265
R_1, wR_2 (all data)	0.0397, 0.0914	0.1159, 0.2602

$^aR_1 = \sum||F_0| - |Fc||/\sum|F_0|$; $wR_2 = \sum[w(F_0^2 - Fc^2)^2]/\sum[w(F_0^2)^2]^{1/2}$.

Table S2. Selected bond lengths (Å) and angels (°) for **JOU-25-R.**

In_1-O_{12}^2	2.131(7)	In_1-O_{25}	2.116(5)
In_1-O_{28}^1	2.125(5)	In_1-O_3^3	2.145(7)
In_1-O_{10}^3	2.178(6)	In_1-O_1	2.188(6)
In_2-O_{25}	2.086(6)	In_2-O_{26}	2.07(6)
In_2-O_2	2.082(6)	In_2-O_{14}	2.15(6)
In_2-O_4^3	2.152(7)	In_2-O_7	2.2(6)
In_3-O_{26}	2.125(6)	In_3-O_{27}	2.115(6)
In_3-O_8	2.115(7)	In_3-O_5^3	2.136(6)
In_3-O_{20}	2.158(6)	In_3-O_{13}	2.16 (6)
In_4-O_{27}	2.068(5)	In_4-O_{28}	2.101(5)
In_4-O_9^3	2.136(6)	In_4-O_{19}	2.152(5)
In_4-O_{11}^1	2.170(6)	In_4-O_6^3	2.17(6)
In_5-O_{29}	2.096(6)	In_5-O_{21}^3	2.163(6)
In_5-O_{15}	2.148(6)	In_5-O_{22}	2.145(6)
In_5-O_{16}^3	2.173(6)	In_5-O_{29}^3	2.09(7)
O_{12}^1-In_1-O_{25}	91.9(6)	O_{12}^1-In_1-O_{28}^2	93.1(6)
O_{25}-In_1-O_{28}^2	90.3(4)	O_{12}^1-In_1-O_3^3	172.3(6)
O_{25}-In_1-O_3^3	93.2(6)	O_{28}^2-In_1-O_3^3	92.7(5)
O_{12}^1-In_1-O_{10}^3	87.4(7)	O_{25}-In_1-O_{10}^3	175.9(5)
O_{28}-In_1-O_{10}^3	93.8(5)	O_3^3-In_1-O_{10}^3	87.1(7)
O_{12}^1-In_1-O_1	86.2(7)	O_{25}-In_1-O_1	93.4(5)
O_{28}^2-In_1-O_1	176.2(5)	O_{33}-In_1-O_1	87. 7(7)
O_{10}^3-In_1-O_1	82.5(5)	O_{25}-In_2-O_{26}	97.2(5)
O_{25}-In_2-O_2	87.3(6)	O_{26}-In_2-O_2	172.5(7)
O_{25}-In_2-O_{14}	97.4(5)	O_{26}-In_2-O_{14}	89.7(5)
O_2-In_2-O_{14}	83.7(7)	O_{25}-In_2-O_4^3	93.4(6)
O_{26}-In_2-O_4^3	93.4(7)	O_2-In_2-O_4^3	92.3(8)

O_{14}-In_2-O_4^3	168.3(7)	O_{25}-In_2-O_7	168.8(5)
O_{26}-In_2-O_7	92.5(5)	O_2-In_2-O_7	83.6(6)
O_{14}-In_2-O_7	88.2(6)	O_4^3-In_2-O_7	80.4(6)
O_{26}-In_3-O_{27}	88.4(5)	O_{26}-In_3-O_8	91(6)
O_{27}-In_3-O_8	91.9(6)	O_{26}-In_3-O_5^3	91(7)
O_{27}-In_3-O_5^5	90.2(6)	O_8-In_3-O_5^3	177.1(7)
O_{26}-In_3-O_{20}	176(6)	O_{27}-In_3-O_{20}	92(5)
O_8-In_3-O_{20}	85(6)	O_5^3-In_3-O_{20}	93(7)
O_{26}-In_3-O_{13}	93(5)	O_{27}-In_3-O_{13}	174.5(5)
O_8-In_3-O_{13}	93.3(7)	O_5^3-In_3-O_{13}	84.5(6)
O_{20}-In_3-O_{13}	86.9(5)	O_{27}-In_4-O_{28}	96.1(5)
O_{27}-In_4-O_9^3	174.2(6)	O_{28}-In_4-O_9^3	87.6(6)
O_{27}-In_4-O_{19}	90.7(5)	O_{28}-In_4-O_{19}	98.4(5)
O_9^3-In_4-O_{19}	84.4(6)	O_{27}-In_4-O_{11}^2	94.9(7)
O_{28}-In_4-O_{11}^2	93.5(6)	O_9^3-In_4-O_{11}^2	89.3(8)
O_{19}-In_4-O_{11}^2	166.3(7)	O_{27}-In_4-O_6^3	92 (5)
O_{28}-In_4-O_6^3	170.1(5)	O_9^3-In_4-O_6^3	84.8(6)
O_{19}-In_4-O_6^3	87.2(6)	O_{11}^2-In_4-O_6^3	80.1(6)
O_{29}-In_5-O_{29}^3	90.6(5)	O_{29}-In_5-O_{21}^3	96.8(7)
O_{29}^3-In_5-O_{21}^3	92.8(7)	O_{29}-In_5-O_{15}	171.3(8)
O_{29}^3-In_5-O_{15}	92.1(7)	O_{21}^3-In_5-O_{15}	91.3(8)
O_{29}-In_5-O_{22}	90.9(7)	O_{29}^3-In_5-O_{22}	172.4(8)
O_{21}^3-In_5-O_{22}	79.6(9)	O_{15}-In_5-O_{22}	87.5(8)
O_{29}-In_5-O_{16}^3	88.3(7)	O_{29}^2-In_5-O_{16}^3	94.2(7)
O_{21}^2-In_5-O_{16}^3	171.3(9)	O_{15}-In_5-O_{16}^3	83.2(9)

Symmetry transformations: ^{1} 1+ x, + y, -1 + z; ^{2} 2 - x,1 - y, -1/2 + z; ^{3} 1 - y, + x - y, 1/3 + z.

Table S3. Selected bond lengths (Å) and angels (°) for **JOU-25-S.**

In_1-O_{26}	2.07(2)	In_1-O_{13}	2.09(3)
In_1-O_{17}^1	2.11(3)	In_1-O_2	2.13(3)
In_1-O_{20}	2.13(3)	In_1-O_{25}	2.17(3)
In_2-O_{19}	2.08(3)	In_2-O_{27}	2.13(3)
In_2-O_{26}	2.15(3)	In_2-O_1	2.15(3)
In_2-O_8	2.18(3)	In_2-O_{16}^2	2.18(3)
In_3-O_{28}^3	2.04(3)	In_3-O_{24}^2	2.08(3)
In_3-O_{27}	2.08(3)	In_3-O_7	2.12(3)
In_3-O_{21}^3	2.16(3)	In_3-O_{15}^2	2.21(3)
In_4-O_{18}^1	2.1(3)	In_4-O_{23}^2	2.1(3)
In_4-O_{25}	2.14(3)	In_4-O_{28}	2.14(3)
In_4-O_{14}	2.15(3)	In_4-O_{22}^3	2.15(3)
In_5-O_{29}^2	2.06(3)	In_5-O_{10}^2	2.11(2)
In_5-O_{29}	2.14(3)	In_5-O_6^3	2.16(3)
In_5-O_9	2.17(3)	In_5-O_5	2.19(3)

O_{26}-In_1-O_{13}	177.1(12)	O_{26}-In_1-O_{17}^1	92.4(12)
O_{13}-In_1-O_{17}^1	90.3(12)	O_{26}-In_1-O_2	91.6(11)
O_{13}-In_1-O_2	85.9(11)	O_{17}^1-In_1-O_2	169.4(13)
O_{26}-In_1-O_{20}	94.6(11)	O_{13}-In_1-O_{20}	86.6(11)
O_{17}^1-In_1-O_{20}	83(12)	O_2-In_1-O_{20}	86.9(12)
O_{26}-In_1-O_{25}	94.3(11)	O_{13}-In_1-O_{25}	84.7(11)
O_{17}^1-In_1-O_{25}	92(12)	O_2-In_1-O_{25}	97.5(12)
O_{20}-In_1-O_{25}	170(11)	O_{19}-In_2-O_{27}	91(11)
O_{19}-In_2-O_{26}	91(11)	O_{27}-In_2-O_{26}	91.8(9)
O_{19}-In_2-O_1	91.2(12)	O_{27}-In_2-O_1	176.2(12)
O_{26}-In_2-O_{14}	83.7(7)	O_{25}-In_2-O_4^3	93.4(6)
O_{26}-In_2-O_1	91.2(11)	O_{19}-In_2-O_8	85.7(12)
O_{27}-In_2-O_8	92.5(11)	O_{26}-In_2-O_8	174.6(10)
O_1-In_2-O_8	84.6(10)	O_{19}-In_2-O_{16}^2	178.2(13)
O_{27}-In_2-O_{16}^2	90.8(12)	O_{26}-In_2-O_{16}^2	88.7(11)
O_1-In_2-O_{16}^2	87(12)	O_8-In_2-O_{16}^2	94.5(12)
O_{28}^3-In_3-O_{24}^2	89.4(11)	O_{28}^3-In_3-O_{27}	98.9(12)
O_{24}^2-In_3-O_{27}	171.2(12)	O_{28}^3-In_3-O_7	97.8(11)
O_{24}^2-In_3-O_7	88.3(12)	O_{27}-In_3-O_7	87.8(11)
O_{28}^3-In_3-O_{21}^3	91.5(11)	O_{24}^2-In_3-O_{21}^3	89.4(12)
O_{27}-In_3-O_{21}^3	93.2(12)	O_7-In_3-O_{21}^3	170.4(13)
O_{28}^3-In_3-O_{15}^2	167.5(11)	O_{24}^2-In_3-O_{15}^2	80.5(11)
O_{27}-In_3-O_{15}^2	91.6(11)	O_7-In_3-O_{15}^2	89.4(12)
O_{21}^3-In_3-O_{15}^2	81(12)	O_{18}^1-In_4-O_{23}^2	83.1(13)
O_{18}^1-In_4-O_{25}	97.3(12)	O_{23}^2-In_4-O_{25}	175.6(12)
O_{18}^1-In_4-O_{28}	94.9(12)	O_{23}^2-In_4-O_{28}	94.9(11)
O_{25}-In_4-O_{28}	89.5(10)	O_{18}^1-In_4-O_{14}	86(13)
O_{23}^3-In_4-O_{14}	84.2(11)	O_{25}-In_4-O_{14}	91.5(11)
O_{28}-In_4-O_{14}	178.6(12)	O_{18}^1-In_4-O_{22}^3	170.2(11)
O_{23}^2-In_4-O_{22}^3	88.6(12)	O_{25}-In_4-O_{22}^3	90.6(12)
O_{28}-In_4-O_{22}^3	91(10)	O_{14}-In_4-O_{22}^3	88(11)
O_{29}^2-In_5-O_{10}^2	90.2(12)	O_{29}^2-In_5-O_{29}	90.8(11)
O_{10}^2-In_5-O_{29}	95.3(12)	O_{29}^2-In_5-O_6^3	95.8(11)
O_{10}^2-In_5-O_6^3	171.2(12)	O_{29}-In_5-O_6^3	91 (13)
O_{29}^2-In_5-O_9	170.5(12)	O_{10}^2-In_5-O_9	80.6(13)
O_{29}-In_5-O_9	92.7(11)	O_6^3-In_5-O_9	93(12)
O_{29}^2-In_5-O_5	94(12)	O_{10}^2-In_5-O_5	90.4(12)
O_{29}-In_5-O_5	172.5(12)	O_6^3-In_5-O_5	82.8(12)

Symmetry transformations: ^{1} 1 + y - x; 1 - x, 1/3 + z; ^{2} 1 - y + x, +x, -1/6 + z; ^{3} 2 - x, 1 -y, 1/2 + z.

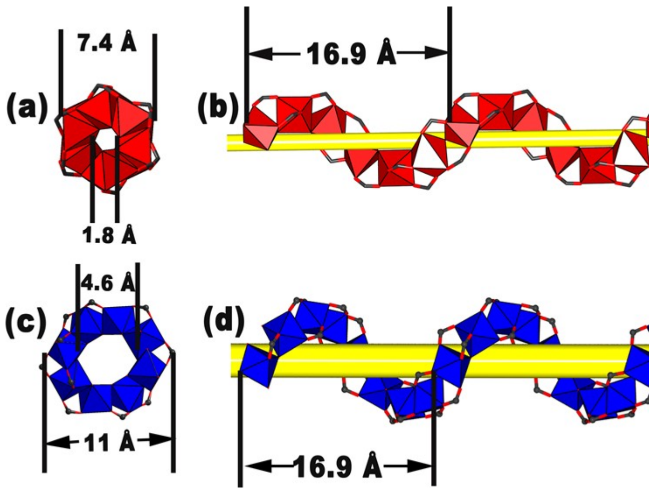

Fig. S1. (a) Outer diameter and inner diameter of **H2** along c axis. (b) The helical distance and angle of **H2** monomer. (c) Outer diameter and inner diameter of **H4** along c axis. (d) The helical distance and angle of **H4** monomer.

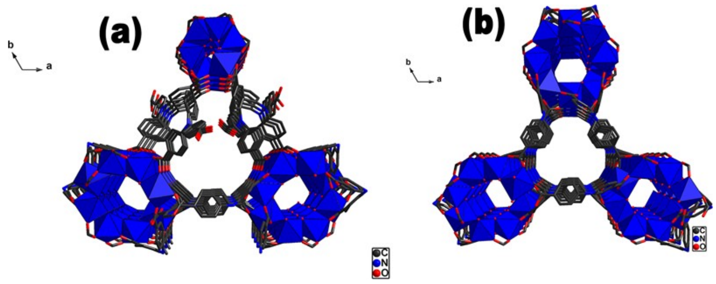

Fig. S2. (a) The structure of small pore along c axis. (b) The structure of large pore along c axis.

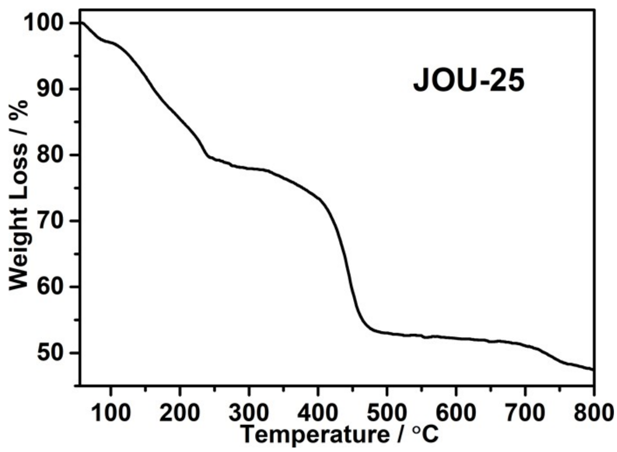

Fig. S3. TG curve of **JOU-25**.

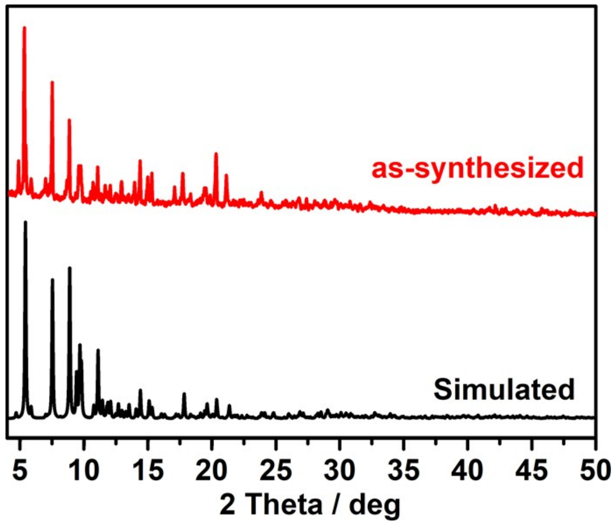

Fig. S4. As-synthesized **PXRD** pattern and simulated spectrum of **JOU-25**.

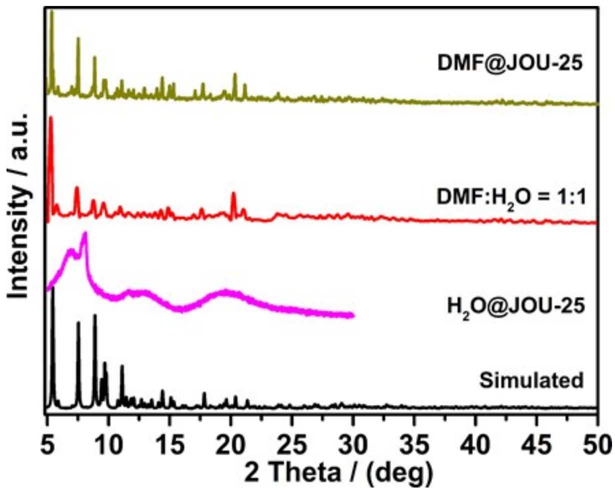

Fig. S5 The stability of **JOU-25** in different solutions.

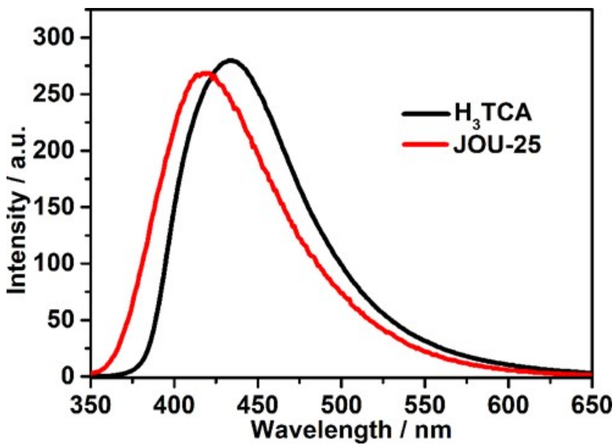

Fig. S6. The fluorescence spectra of **JOU-25** and H_3TCA in mixed solution of DMF/H_2O (V/V = 1:1).

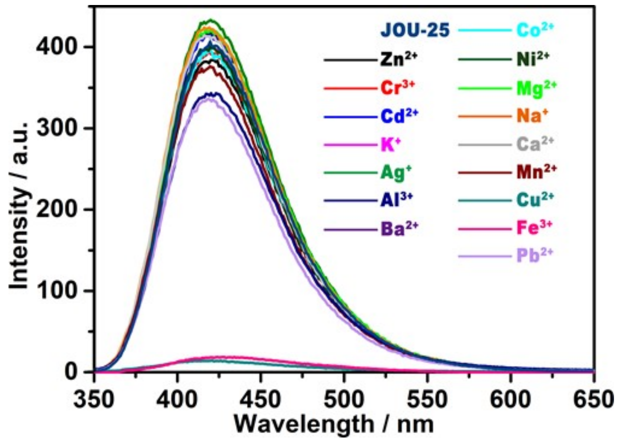

Fig. S7. Emission spectra of **JOU-25** in DMF solution in the presence of different metal ions.

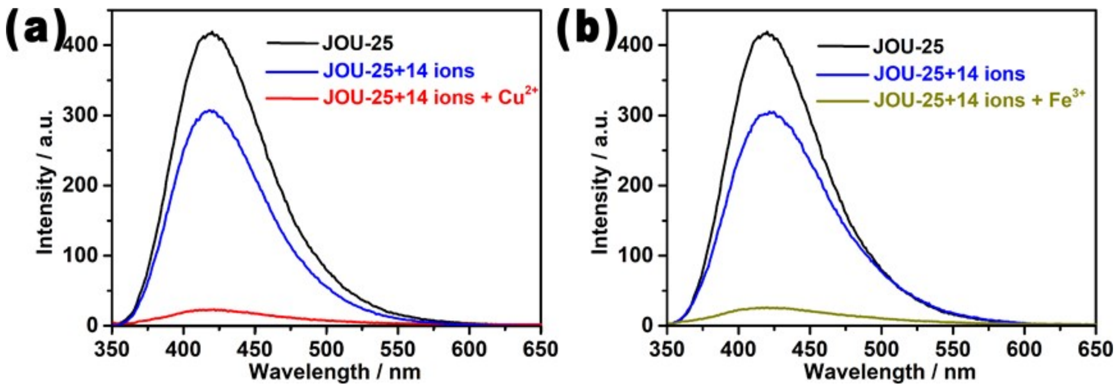

Fig. S8. (a) Emission spectra of **JOU-25** in DMF/H_2O solution with different concentration of Cu^{2+}. (b) Emission spectra of **JOU-25** in DMF/H_2O solution with different concentration of Fe^{3+}.

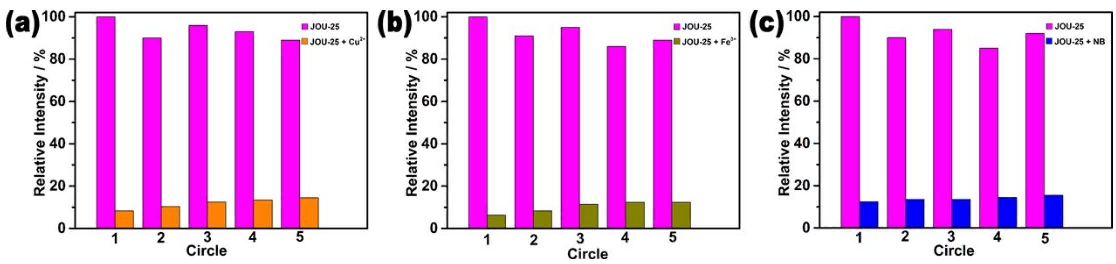

Fig. S9. (a) The recyclability test of **JOU-25** regarding Cu^{2+} detection. (b) The recyclability test of **JOU-25** regarding Fe^{3+} detection. (c) The recyclability test of **JOU-25** regarding NB detection. Magenta column: luminescent intensity of **JOU-25** dispersion before adding detected molecules; orange column: the relative luminescent intensity after adding Cu^{2+} solution; green column: the relative luminescent intensity after adding Fe^{3+} solution; blue volume: the relative luminescent intensity after adding NB solution.

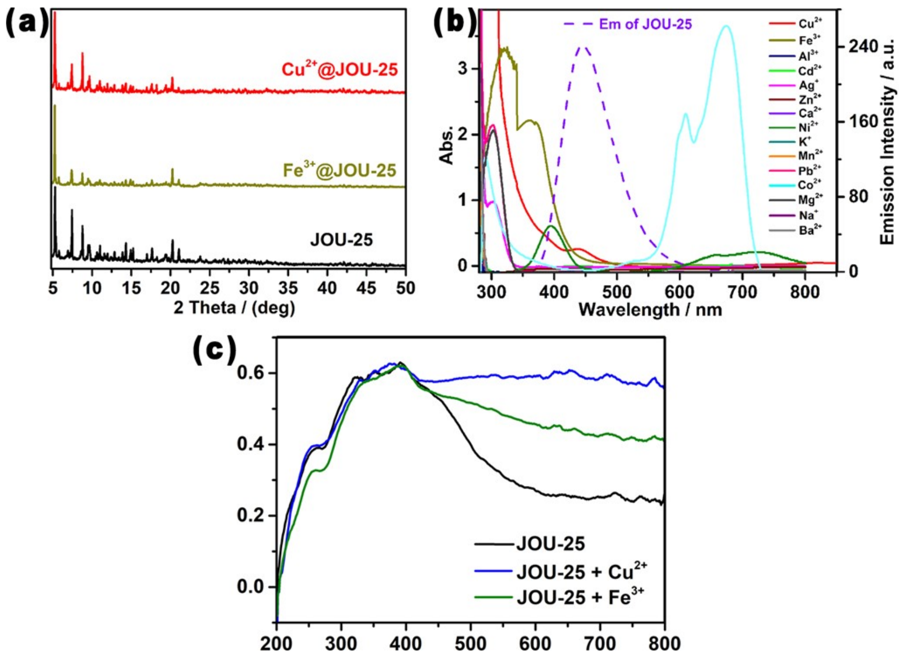

Fig. S10. (a) Stability of **JOU-25** after releasing Cu^{2+}/Fe^{3+}. (b) UV-Vis absorption spectra of metal ions and emission spectra of **JOU-25**. (c) The solid UV-Vis absorption spectra of **JOU-25**, Cu^{2+}@**JOU-25** and Fe^{3+}@**JOU-25**.

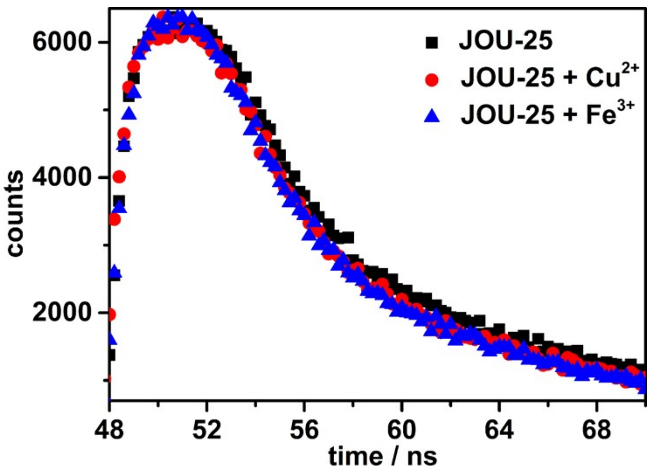

Fig. S11. Fluorescence decay curves of **JOU-25**, **JOU-25** + Fe^{3+} and **JOU-25** + Cu^{2+}.

Table S4 Comparison of reported MOF sensors for Cu^{2+} ion detection.

MOFs	K_{SV} (M^{-1})	**Detection limit (M^{-1})**	**Ref.**
JOU-25	392867	3.82×10^{-7}	This work
$Cd(INA)(pytpy)(OH)\cdot 2H_2O$	130000	3.05×10^{-6}	4
UiO-66-$(COOH)_2$	41200	2.3×10^{-7}	5
MIL-53-L	6150	-	6
$[Cd(L)_2]\cdot(DMF)_{0.92}$	4430	7×10^{-5}	7
$[Tb_3(L)_2(HCOO)(H_2O)_5]\cdot DMF\cdot 4H_2O$	2021.8	1×10^{-6}	8

Table S5 Comparison of reported MOF sensors for Fe^{3+} ion detection.

MOFs	K_{SV} **(M^{-1})**	**Detection limit (M^{-1})**	**Ref.**
Bi-TCBPE	578000	9.8×10^{-7}	9
JOU-25	313907	3.82×10^{-7}	This work
Eu-MOF	20280	4×10^{-5}	10
Tb-MOF	16590	-	11
UiO-66-NDC	16000	6.5×10^{-7}	12
$[Tb_{10}(DBA)_6(OH)_4(H_2O)_5]\cdot(H_3O)_4$	9580	1×10^{-9}	13
$[Zn(oba)(L)_{0.5}]\cdot dma$	9300	-	14
Eu-MOF/ALD-PPS	4366	5.4×10^{-6}	15

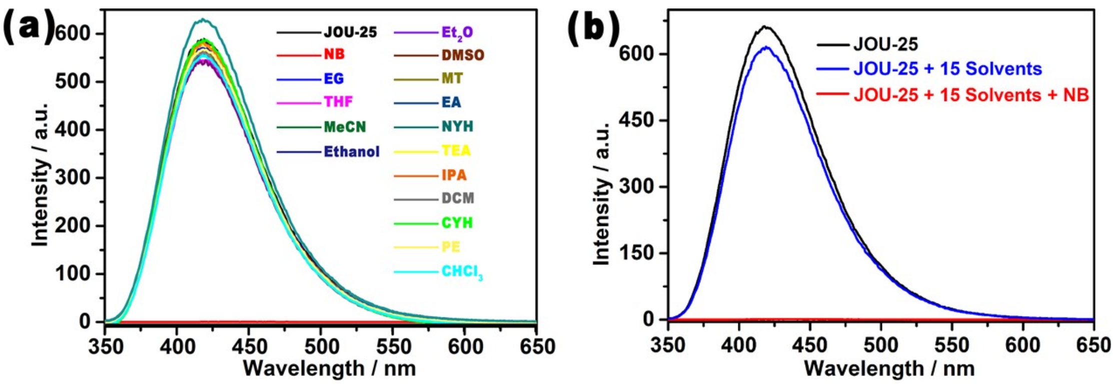

Fig. S12. (a) Emission spectra of **JOU-25** in DMF solution in the presence of different organic solvents. (b) Emission spectra of **JOU-25**, **JOU-25** + 15 organic solvents and **JOU-25** + 15 solvents + NB in DMF/H_2O solution.

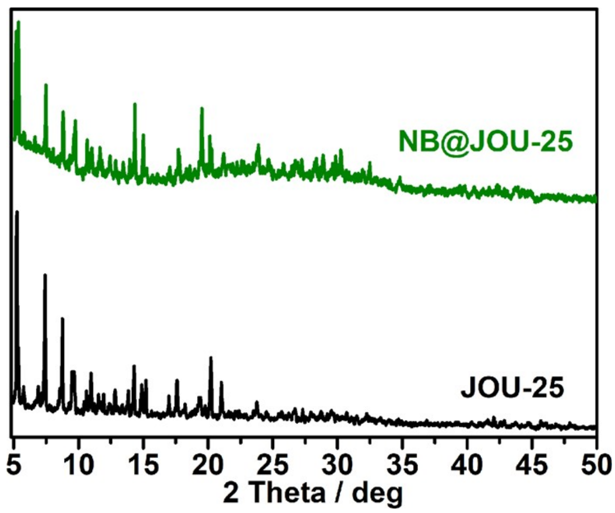

Fig. S13. Stability of **JOU-25** after releasing NB.

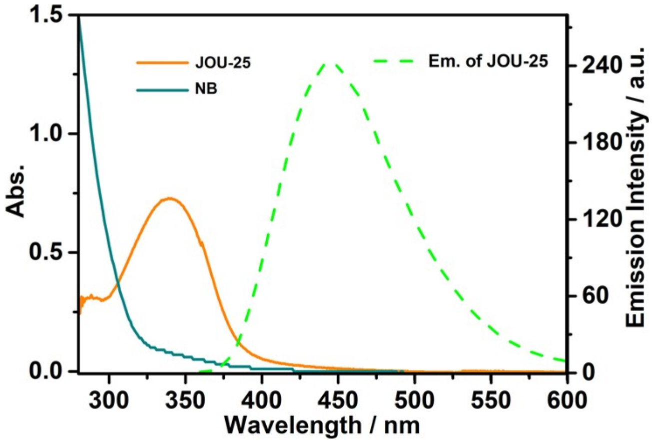

Fig. S14. UV-Vis absorption spectra of NB and **JOU-25**, and emission spectrum of **JOU-25.**

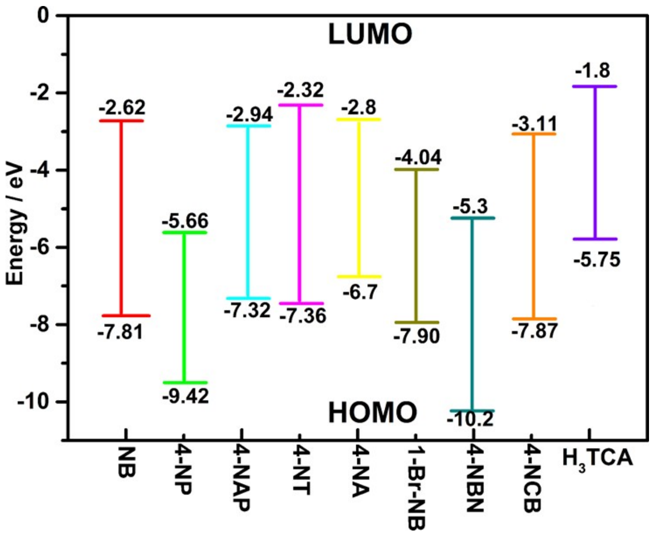

Fig. S15. The LUMO and HOMO energy levels of H_3TCA and NACs.

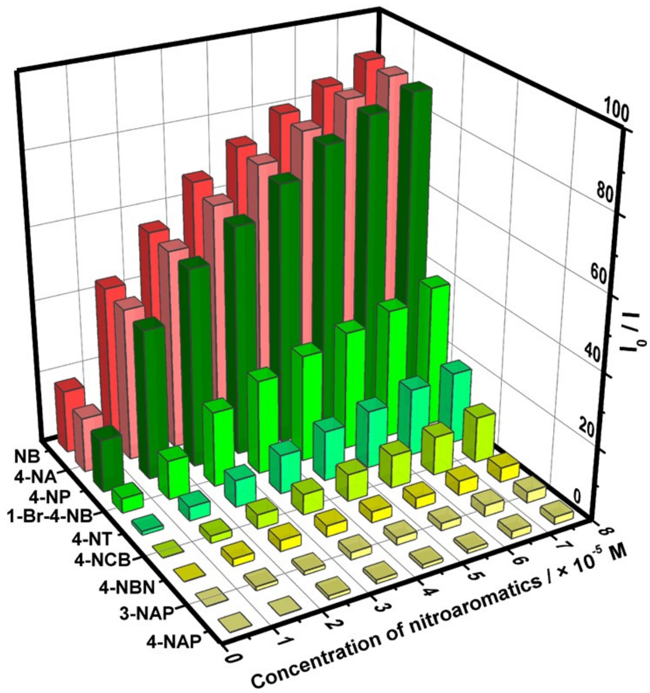

Fig. S16. Emission quenching percentage of **JOU-25** dispersion with different nitroaromatics.

Table S6. Comparison of reported MOF sensors for NB detection.

MOFs	K_{SV} (M^{-1})	Detection limit (M^{-1})	Quenching efficiency (%)	Ref.
FJU-35	1630000	-	43	16
FJU-36	913000	-	49	16
JOU-25	49803	2.41×10^{-6}	90	**This work**
In/Eu-CBDA	16900	8.88×10^{-6}	82	17
$[Cu(L)(I)]_2 \cdot 2DMF \cdot MeCN$	9500	6.6×10^{-6}	40	18
$[Cd(bipy)][HL]_n$	9300	-	100	19
Ln-MOFs	3340	2.89×10^{-5}	100	20
Cd-MOF	2700	2.54×10^{-3}	100	21

Reference

1. Nandi, S.; Chakraborty, D.; Vaidhyanathan, R., A permanently porous single molecule H-bonded organic framework for selective CO_2 capture. *Chem. Commun.* 52 (2016) 7249-7252.
2. Sheldrick, G. M., Crystal structure refinement with SHELXL. *Acta. Crystallogr. C.* 71 (2015) 3-8.
3. Kim, H. C.; Huh, S.; Lee, D. N.; Kim, Y., Selective carbon dioxide sorption by a new breathing three-dimensional Zn-MOF with Lewis basic nitrogen-rich channels.

Dalton Trans. 47 (2018) 4820-4826.
4. Zhang, J.; Wu, J.; Tang, G.; Feng, J.; Luo, F.; Xu, B.; Zhang, C., Multiresponsive water-stable luminescent Cd coordination polymer for detection of TNP and Cu^{2+}. *Sensor. Actuat. B-Chem.* 272 (2018) 166-174.
5. Peng, X. X.; Bao, G. M.; Zhong, Y. F.; He, J. X.; Zeng, L.; Yuan, H. Q., Highly selective detection of Cu(2+) in aqueous media based on Tb(3+)-functionalized metal-organic framework. *Spectrochim. Acta. A.* 240 (2020) 118621.
6. Liu, C.; Yan, B., A novel photofunctional hybrid material of pyrene functionalized metal-organic framework with conformation change for fluorescence sensing of Cu^{2+}. *Sensor. Actuat. B-Chem.* 235 (2016) 541-546.
7. Senthilkumar, S.; Goswami, R.; Smith, V. J.; Bajaj, H. C.; Neogi, S., Pore wall-functionalized luminescent Cd(II) framework for selective CO_2 adsorption, highly specific 2,4,6-trinitrophenol detection, and colorimetric sensing of Cu^{2+} ions. *ACS. Sustain. Chem. Eng.* 6 (2018) 10295-10306.
8. Zhao, J.; Wang, Y. N.; Dong, W. W.; Wu, Y. P.; Li, D. S.; Zhang, Q. C., A robust luminescent Tb(III)-MOF with lewis basic pyridyl dites for the highly sensitive detection of metal ions and small molecules. *Inorg. Chem.* 55 (2016) 3265-3271.
9. Guan, Q. L.; Han, C.; Bai, F. Y.; Liu, J.; Xing, Y. H.; Shi, Z.; Sun, L. X., Bismuth-MOF based on tetraphenylethylene derivative as a luminescent sensor with turn-off/on for application of Fe^{3+} detection in serum and bioimaging, as well as emissive spectra analysis by TRES. *Sensor. Actuat. B-Chem*. 325 (2020) 128767.
10. Yu, H.; Fan, M.; Liu, Q.; Su, Z.; Li, X.; Pan, Q.; Hu, X., Two highly water-stable imidazole-based Ln-MOFs for sensing Fe(3+),Cr_2O_7(2-)/CrO4(2-) in a water environment. *Inorg. Chem.* 59 (2020) 2005-2010.
11. Zhang, Q.; Wang, J.; Kirillov, A. M.; Dou, W.; Xu, C.; Xu, C.; Yang, L.; Fang, R.; Liu, W., Multifunctional Ln-MOF luminescent probe for efficient sensing of Fe(3+), Ce(3+), and acetone. *ACS. Appl. Mater. Inter.* 10 (2018) 23976-23986.
12. He, Y.; Shi, L.; Wang, J.; Yan, J.; Chen, Y.; Wang, X.; Song, Y.; Han, G., UiO-66-NDC (1,4-naphthalenedicarboxilic acid) as a novel fluorescent probe for the selective detection of Fe^{3+}. *J. Solid. State. Chem.* 285 (2020) 121206.
13. Chai, H. M.; Zhang, G. Q.; Jiao, C. X.; Ren, Y. X.; Gao, L. J., A multifunctional Tb-MOF detector for H_2O_2, Fe(3+), Cr_2O_7(2-), and TPA explosive featuring coexistence of binuclear and tetranuclear clusters. *ACS. Omega*. 5 (2020) 33039-33046.
14. Chand, S.; Pal, A.; Pal, S. C.; Das, M. C., A trifunctional luminescent 3D microporous MOF with potential for CO_2 separation, selective sensing of a metal ion, and recognition of a small organic molecule. *Eur. J. Inorg. Chem.* 2018 (2018) 2785-2792.
15. Yu, Y.; Pan, D.; Qiu, S.; Ren, L.; Huang, S.; Liu, R.; Wang, L.; Wang, H., Polyphenylene sulfide paper-based sensor modified by Eu-MOF for efficient detection of Fe^{3+}. *React. Funct. Polym*. 165 (2021) 104954.
16. Liu, L.; Yao, Z.; Ye, Y.; Chen, L.; Lin, Q.; Yang, Y.; Zhang, Z.; Xiang, S., Robustness, selective gas separation, and nitrobenzene sensing on two isomers of cadmium metal-organic frameworks containing various metal-O-metal chains. *Inorg. Chem. 2018*, 57 (20), 12961-12968.

17. Zhang, Y.; Ying, Y.; Feng, M.; Wu, L.; Wang, D.; Li, C., Two isostructural Ln^{3+}-based heterometallic MOFs for the detection of nitro-aromatics and $Cr_2O_7^{2-}$. *New. J. Chem.* 44 (2020) 12748-12754.
18. Sajal Khatua, S. G., Soumava Biswas,; Kapil Tomar, H. S. J., Sanjit Konar, A stable multi-responsive luminescent MOF for colorimetric detection of small molecules in selective and reversible manner. *Chem. Mater.* 27 (2015) 5349-5360.
19. Kan, W.-Q.; Wen, S.-Z., A fluorescent coordination polymer for selective sensing of hazardous nitrobenzene and dichromate anion. *Dyes. Pigments.* 139 (2017) 372-380.
20. Du, Y.; Yang, H.; Liu, R.; Shao, C.; Yang, L., A multi-responsive chemosensor for highly sensitive and selective detection of Fe(3+), Cu(2+), Cr2O7(2-) and nitrobenzene based on a luminescent lanthanide metal-organic framework. *Dalton. Trans.* 2020, 49 (37), 13003-13016.
21. Yan, Y.-T.; Liu, J.; Yang, G.-P.; Zhang, F.; Fan, Y.-K.; Zhang, W.-Y.; Wang, Y.-Y., Highly selective luminescence sensing for the detection of nitrobenzene and Fe^{3+} by new Cd(ii)-based MOFs. *CrystEngComm* 20 (2018) 477-486.